2014 IEEE International Conference on Robotics & Automation (ICRA)
Hong Kong Convention and Exhibition Center
May 31 - June 7, 2014. Hong Kong, China

Characterization of Three-dimensional Steering for Helical Swimmers

Tiantian Xu[1], Gilgueng Hwang[2], Nicolas Andreff[3] and Stéphane Régnier[1]

Abstract— **Helical microswimmers capable of propulsion at low Reynolds numbers have been proposed for many applications. However, closed-loop controlled helical swimmers are still challenging because of the limits of optical tracking, and a lack of control parameters lying on the swimming characteristics of both linear propulsion and steering. Although the linear propulsion characteristics of helical swimmers were extensively studied, the steering characteristics have not yet been clearly shown. Helical microswimmers are efficient in propulsion, whereas their high surface-to-volume ratio limits the steering performances. In this paper, we characterized both the direction and inclination steering using a real-time visual tracking of orientation. The direction steering efficiency could be increased in terms of response time with a higher inclination angle both in floating conditions and on a sticky substrate. We thus developed a 3D steering strategy by combining direction and inclination steering to improve the steering performance. We further expect that the characterization of steering performance can contribute to defining the control parameters for future closed-loop control.**

I. Introduction

Helical microrobots capable of propulsion at low Reynolds number have been proposed for numerous applications ranging from in vitro tasks on lab-on-a-chip (e.g. transporting and sorting micro objects [1], [2], [3]; mechanical components micro assembly [4]...) to in vivo applications for minimally invasive medicine (e.g. targeted drug delivery; brachytherapy; hyperthermia [5], [6]...), due to their micro sizes and accessibility to tiny and clustered environments.

Helical propellers inspired by E.coli bacterial swimming behaviors are promising for swimming at low Reynolds numbers, because helical propulsion is non-reciprocal motion [7], [8], [9]. An E.coli bacterium consists of a rod-shaped head and a bundle of passive flagella driven by a rotary motor into a helical shape to generate a corkscrew-like motion [10]. Therefore, a rigid helical tail fixed to a magnetic head or a magnetic-coated helical tail actuated by a rotating magnetic field, which convert rotary motion to linear motion, are approaches to propulsion at low Reynolds numbers.

Since recent decades, researchers have developed several different magnetically actuated helical swimmers. Honda [11] and Ishiyama [12] proposed the first magnetically actuated helical swimmers. The first helical swimmers, overall several centimetres long, could swim linearly in viscous liquid or soft tissue. Bell fabricated micron-sized helical swimmers, by using a self-scrolling fabrication technique which relies on the controlled internal stress of thin GaAs/InGaAs bilayers [13]. Zhang then characterized their linear propulsion properties [14], [15]. By deviating the plane of the rotating field, the helical swimmer would reorient itself to become perpendicular again to the plane of the rotating field. The steering both in the horizontal and vertical planes was tested. Ghosh fabricated an even smaller helical swimmer with a length of 2 μm, using glancing angle deposition (GLAD) [16]. This helical swimmer could follow a curved trajectory, for example "R@H", under the action of a preprogrammed magnetic field. This curved trajectory was not parametrized. Hwang proposed a helical swimmer actuated by electro-osmosis force with an overall length of 74 μm [17], [18]. These helical swimmers were pulled by electrical gradient and showed high swimming performance. The steering was realized by the gradient direction which was different from magnetically actuated helical swimmers. Mahoney showed open-loop controlled swimming of a helical swimmer with an overall length of 5 mm, which enabled a "U-turn" trajectory in the vertical plane [19]. He proposed a method to calculate the inclination angle of the helical swimmer with the horizontal plane, so that the helical swimmer could generate a propulsion force in the upward direction to compensate its own gravity. Tottori fabricated helical swimmers ranging from 4 μm to 64.5 μm using 3D direct laser writing (DLW) [3]. The helical swimmers enabling 3D motion could carry a sphere as well as raise it up.

However, closed-loop controlled helical swimmers are still challenging because of several reasons such as the limits of optical tracking, and lack of control strategies. The control strategy lies on the swimming characterizations of both linear propulsion and steering. Although the linear propulsion was extensively studied, the steering has never been characterized. In this paper, we characterized the steering of a helical swimmer using a real-time orientation visual tracking method, including steering of direction and inclination angle. We later compared the performances of direction steering with different inclination angles by their response times to step angle steering commands. We thus proposed a 3D steering strategy by combining inclination and direction steering to improve the steering performance. Finally, we characterized the direction steering and tested the proposed strategy on a sticky substrate to simulate high surface friction at the microscale.

In this paper, Section II defines the direction and inclination angles of the helical swimmer. Compared to our previous works [20], [21], we designed a new helical swimmer and developed Helmholtz coils for uniform rotating magnetic

[1]T.XU and S.Régnier are with ISIR - Institut des Systèmes Intelligents et Robotique, UPMC, Paris, France. tiantian.xu@isir.upmc.fr, stephane.regnier@upmc.fr

[2]G. Hwang is with Laboratoire de Photonique et de Nanostructures, Marcoussis, France. gilgueng.hwang@lpn.cnrs.fr

[3]N. Andreff is with FEMTO-ST Institute, UFC, Besançon, France. nicolas.andreff@femto-st.fr

field generation in Section III. The real-time visual tracking of the helical swimmer's axis is also introduced in this section. Section IV shows the direction and inclination steering characteristics of the helical swimmer. The steering performances respectively in floating conditions and on a sticky substrate are compared in this section.

II. Modelling of Magnetically Actuated Helical Swimmer Steering

A. Magnetic force and torque

All magnetized objects are exerted both force and torque within an externally imposed magnetic field. The magnetic force and torque induced on a magnetized object are expressed as follows [22]:

$$\overrightarrow{f_m} = \int_{V_m} (\overrightarrow{M} \cdot \bigtriangledown) \overrightarrow{B} \, \mathrm{d}V_m \tag{1}$$

$$\overrightarrow{\tau_m} = \int_{V_m} \overrightarrow{M} \times \overrightarrow{B} \, \mathrm{d}V_m \tag{2}$$

where V_m is the volume of the magnetized object, $\overrightarrow{B}$ is the flux density of the applied field (T), $\overrightarrow{M}$ is the magnetization of the object $(\mathrm{A/m})$. The magnetic field to actuate the helical swimmer is considered as uniform. There is no magnetic force exerted on the helical swimmer.

B. Inclination angle and direction angle

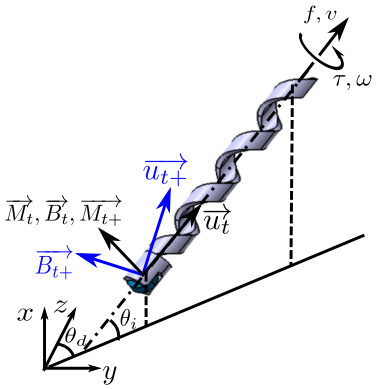

Fig. 1: Magnetic helical swimmer steering model. The inclination angle and direction angle of steering are respectively θ_i and θ_d.

The inclination angle θ_i is defined as the angle between the axis of helical swimmer and the horizontal plane yOz, as shown in Fig. 1. This inclination angle is very important to control the height of the helical swimmer. The propulsive force projected to the upward direction can be increased by increasing the inclination angle or rotation frequency. If the propulsive force created by the helical swimmer projected on the upward direction is higher than its own gravity, the helical swimmer will go upwards. Otherwise, the helical swimmer will go downwards.

The direction angle θ_d is defined as the angle between the z axis and the projection of the helical swimmer axis on the horizontal plane, as shown in Fig. 1. By controlling the direction angle of the helical swimmer, we can control its forward direction projected on the horizontal plane.

C. Modelling of steering

At the equilibrium regime, the helical swimmer rotates synchronously with the external rotating magnetic field around $\overrightarrow{u_t}$. The axis direction of the SHM should be in the direction of $\overrightarrow{u_t}$. The magnetization of the SHM is noted as $\overrightarrow{M_t}$, and the magnetic field is noted as $\overrightarrow{B_t}$. Both $\overrightarrow{M_t}$ and $\overrightarrow{B_t}$ are perpendicular to the axis $\overrightarrow{u_t}$. The magnetic torque exerted on the SHM τ_t can be expressed as:

$$\overrightarrow{\tau_t} = \overrightarrow{M_t} \times \overrightarrow{B_t} \tag{3}$$

should be also in the direction of $\overrightarrow{u_t}$, which keep the SHM rotating around $\overrightarrow{u_t}$.

At time t, the axis of the rotating magnetic field changes to $\overrightarrow{u_{t+}}$. The magnetic field $\overrightarrow{B_{t+}}$ becomes perpendicular to $\overrightarrow{u_{t+}}$. However, the magnetization of the SHM $\overrightarrow{M_{t+}}$ is still perpendicular to the initial axis $\overrightarrow{u_t}$. The magnetic torque $\overrightarrow{\tau_{t+}}$ exerted on the SHM after the axis change of the rotating magnetic field can be now expressed as:

$$\overrightarrow{\tau_{t+}} = \overrightarrow{M_{t+}} \times \overrightarrow{B_{t+}} \tag{4}$$

where the magnetic field can be decomposed in the directions perpendicular and parallel to the direction of $\overrightarrow{u_t}$. Then, the magnetic field $\overrightarrow{B_{t+}}$ can be expressed as:

$$\overrightarrow{B} = \overrightarrow{B_{\perp u_t}} + \overrightarrow{B_{\parallel u_t}} \tag{5}$$

Therefore, the magnetic torque exerted on the SHM after the axis of the rotating magnetic field changes can then be written as:

$$\overrightarrow{\tau_{t+}} = \underbrace{\overrightarrow{M_{t+}} \times \overrightarrow{B_{\perp u_t}}}_{\overrightarrow{\tau_{\parallel u_t}}} + \underbrace{\overrightarrow{M_{t+}} \times \overrightarrow{B_{\parallel u_t}}}_{\overrightarrow{\tau_{\perp u_t}}} \tag{6}$$

As the magnetization $\overrightarrow{M_{t+}}$ is perpendicular to the $\overrightarrow{u_t}$ direction, this magnetic torque can be decomposed in the directions perpendicular and parallel to $\overrightarrow{u_t}$ as well. The torque $\overrightarrow{\tau_{\parallel u_t}}$ is the magnetic torque in the direction of $\overrightarrow{u_t}$, which makes the SHM rotate around its actual axis $\overrightarrow{u_t}$. The magnetic torque $\overrightarrow{\tau_{\perp u_t}}$ is the magnetic torque perpendicular to $\overrightarrow{u_t}$, which makes the SHM rotate around the direction of $\overrightarrow{u_t} \times \overrightarrow{M_t}$. That means the direction of the axis of the SHM changes. The axis direction change of the SHM is called the 3D steering of the SHM.

III. System Overview

A. Magnetic actuation system

We developed three orthogonally arranged Helmholtz coil pairs to generate an uniform rotating field. Each Helmholtz coil pair generates the uniform magnetic field in one direction. As shown in Fig. 2a, the axis of small coils is x, the axis of medium coils is y, and the axis of big coils is z. The Helmholtz coils are designed for a maximum field strength generation of 10 mT. The specifications of the three coil pairs are depicted in Table I.

TABLE I: Specifications of 3 orthogonal arranged Helmholtz coil pairs design.

	Radius (mm)	Nb of turns	Witch (mm)	Thickness (mm)
Small	50	500	24	13.3
Medium	80	600	24	16
big	110	600	24	16

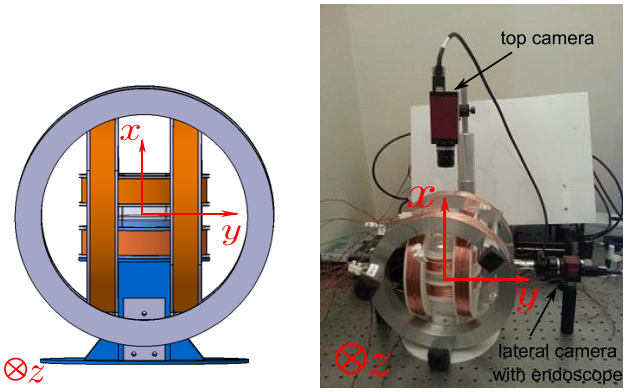

(a) (b)

Fig. 2: (a) Three orthogonal Helmholtz coil pairs CAD design with corresponding axes. (b) System setup: Helmholtz coils, top camera, side camera with endoscope.

Each set of Helmholtz coils is driven by an ADS 50/5 4-Q-DC servoamplifier of Maxon Motor Control amplifier, capable of 5 A continuous current and 10 A peak current. The amplifiers are alimented by a TDK-Lambda SWS300-48 DC power supply, capable of 6.7 A current. The output tension of the power supply is 48 V. The amplifiers are used on current control mode, the output currents are thus constant. Analog communication between the PC and the amplifiers is accomplished with a Sensoray 626 Analog and Digital I/O card. The magnetic fields generated by three coil pairs were measured and calibrated by a gaussmeter Hirst GM08.

Two cameras were used. As shown in Fig. 2b, one was on the top, while the other was beside the Helmholtz coils. The direction angle of the helical swimmer was detected by a firewire camera on the top (Pike F032B), through the opening on the top of the Helmholtz coils. The inclination angle was detected by a side camera (Guppy Pro F032). Due to the limited side opening, an endoscope (Bipol) with diameter of 2.7 mm was mounted on the camera instead of a simple lens. The angle tracking method will be introduced in III-D. The videos were recorded at 25 frames per second.

B. Magnetic actuated helical swimmer in viscous liquid

We designed a helical swimmer with a magnetic head to characterize steering performances. The helical swimmer were made of resin by *3d prod* (*http://www.3dprod.com/*), as shown in Fig. 3b. The advantages of the resin helical swimmer are the low cost and the quick fabrication. The helical swimmer is black in order to have a good image contrast for tracking. The helical swimmer has an overall length of 17.8 mm with 3.5 turns. The length of each pitch is 4 mm. The width of the helical tail is 1.4 mm. The thickness of the helical swimmer is 0.3 mm. A permanent magnet with diameter of 1.5 mm and 0.5 mm thick was set in the head. The magnet is magnetized in the direction of the diameter, so that the helical swimmer will rotate around its own axis in a rotating magnetic field.

(a) (b) (c)

Fig. 3: (a) CAD design of the helical swimmer with a magnetic head. (b) The fabricated helical swimmer viewed by the top camera. (c) The helical swimmer tracked by ViSP. The red cross is the online calculated barycentre and the red line is the online calculated axis of the helical swimmer.

C. Reynolds numbers and cut-off frequency

The magnetically actuated helical swimmers with a magnetic head show a cut-off frequency [21]. Below the cut-off frequency, the helical swimmer rotates in sync with the external rotating magnetic field. Beyond this cut-off frequency, the rotation frequency of the helical swimmer decreases. The cut-off frequency depends on the Reynolds number.

In the following experiments, the helical swimmer is put in pure glycerol liquid. The glycerol density, which is 1.26×10^3 kg/m^3, was measured by a portable density meter (DMA 35). The viscosity of glycerol at about 23 °C was measured by a falling ball viscometer (Brookfield KF10), which yielded 1350 mPa·s. The helical swimmer used in the experiments swims at 0.1 mm/s to 0.5 mm/s. The calculated Reynolds number is $0.001 - 0.008$. Swimming at $Re \ll 1$ is defined as swimming at low Reynolds numbers. Therefore, the helical swimmer swims at low Reynold numbers in the following experiments. The cut-off frequency of the helical swimmer in the pure glycerol is 5 Hz. In the following experiment, the magnetic field rotation frequency is below the cut-off frequency. The helical swimmer is supposed to rotate synchronously with the magnetic field.

D. Helical swimmer tracking and axis calculation

A robust extraction and real-time tracking of the helical swimmer is important for steering performance characterization and eventually for visual servoing tasks. The tracking of the helical swimmer in the following experiments was realised by ViSP [23]. The helical swimmer is considered as a blob (vpDot class in ViSP) in images, defined by a set of connected pixels with the same gray level. The helical swimmer viewed by the top camera is shown in Fig. 3b, and the helical swimmer tracked by ViSP is presented in Fig. 3c in green.

The barycentre and the axis of a helical swimmer can be calculated from image moments. The general 2D $(p+q)^{th}$ order moments of a grey-level image $f(x,y)$ are defined as [24]:

$$m_{pq} = \iint_I x^p y^q f(x,y)\,\mathrm{d}x\mathrm{d}y \tag{7}$$

with $p,q = 0,1,2...$

The barycentre of an object is defined as the center of mass of a figure of the same shape with constant mass per unit area. The center of the mass, in turn, is that point where all the mass of the object could be concentrated without changing the first moment of the object about any axis. Therefore, the barycentre of the helical swimmer $(\bar{x},\bar{y})$ can be expressed by:

$$(\bar{x},\bar{y}) = \left(\frac{m_{10}}{m_{00}}, \frac{m_{01}}{m_{00}}\right) \tag{8}$$

which is presented in Fig. 3c by red cross.

The orientation of a object in the image can be defined by the direction of the axis of least inertia. It means that the line for which the integral of the square of the distance to points in the object is a minimum. From this, the angle θ between the axis of the helical swimmer and the u axis of the image can be expressed by [24]:

$$\tan 2\theta = \frac{b}{(a-c)} \tag{9}$$

with

$$a = \frac{m_{21}}{m_{00}} - \bar{x}^2 \tag{10}$$

$$b = 2\left(\frac{m_{11}}{m_{00}} - \overline{xy}\right) \tag{11}$$

$$c = \frac{m_{02}}{m_{00}} - \bar{y}^2 \tag{12}$$

Thanks to the calculated barycentre and the orientation of the helical swimmer, its axis can be drawn by a line passing by its barycentre and with a slope of θ, which is presented in Fig. 3c.

IV. Steering Characterization of Helical Swimmer

In this section, we characterize the steering by the helical swimmer orientation response to a step angle steering command. The steering performance refers to the response time to a step angle steering command. The response time is defined as the time that a helical swimmer uses to establish a steady state regime from the step angle steering command.

A. Direction steering characterization

The direction steering of the helical swimmer was characterized with different inclination angles (0°, 45°, and 65°). The direction angle of the helical swimmer was detected by the top camera, and the inclination angle was monitored by the side camera. The helical swimmer was initially floating in the liquid with a direction angle of 0°. The rotation frequency of the helical swimmer was 3 Hz. The clockwise direction is defined as the positive direction of steering. At the end of 2 s, the axis of the rotating magnetic field was changed to give a steering command.

1) Inclination angle of 0°: It is well-known that, with the inclination angle of 0°, if the direction angle changes by 180°, the helical swimmer will just reverse its rotation direction to reverse the advance direction. However, the position of the head relative to its body does not change. In other words, the head can not be always kept in the front of or at the back of the helical swimmer.

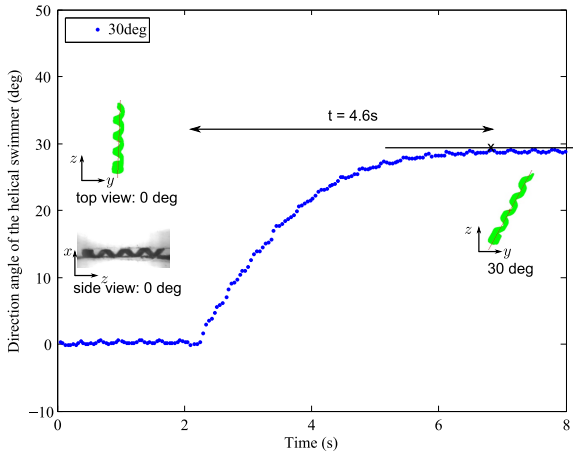

Fig. 4: Step response to the 30° direction steering with a 0° inclination angle.

The step response to small angle steering, such as a 30° angle, is shown in Fig. 4. The response shows first order system characteristics. The response time is 4.6 s. The magnetic torque is not high enough to steer the helical swimmer direction with 90°. The helical swimmer stopped its self-rotation, because its axis was no longer along the axis of the rotating magnetic field. The direction of the helical swimmer's axis stayed at 0°.

An oscillation of 3 Hz appeared, which was caused by the dissymmetry of helical morphology relative to its axis. The oscillation could allow to analyse the phase of the helical swimmer in its self-rotation.

2) Inclination angle of 45°: Then, the helical swimmer was inclined up with an inclination angle of 45°. The direction steering at 30°, 90°, 180°, and −90° angles were respectively studied. The step responses of steering are shown in Fig. 5. After a 180° angle direction steering with 45° inclination angle, not only the advance direction, but also the head position changed. The head stayed at the back of the helical swimmer no matter what the advance direction was. The 90° angle direction steering can be easily achieved with a 45° inclination angle. Compare to 0° inclination angle, less energy is required for a 90° angle direction steering. The energy efficiency increased with the inclination angle. The response times are summarized in Table II. It shows that the steering performance is improved in terms of response time by inclining the helical swimmer at 45°.

The responses to the 30°, −90°, and 180° angle direction

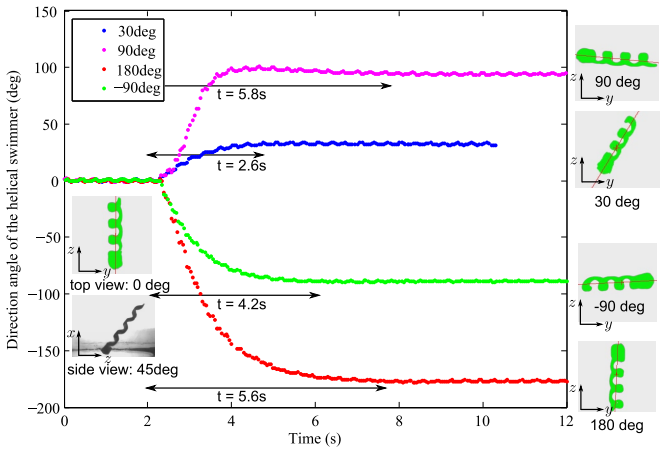

Fig. 5: Step responses of 30°, 90°, 180°, and −90° angle direction steering with a 45° inclination angle.

TABLE II: Response times of direction steering of the helical swimmer with different inclination angles (unit: s).

Inclination angle	Command angle of direction steering			
	30°	90°	180°	−90°
0°	4.6	∞	-	∞
45°	2.6	5.8	5.6	4.2
65°	2.3	4.4	4.8	3.5

steering show first order system characteristics. However, the 90° angle direction steering shows second order system characteristics. Fig. 6 and 7 depict the images sequences of 90° and −90° angle direction steering respectively from the top camera and side camera. From the apparent length of the helical swimmer in the top view, we deduced that the inclination angle of the helical swimmer did not change during the −90° angle steering, but increased during the 90° angle steering. It was caused by the inertia of the helical swimmer self-rotation, which was in the counter clockwise direction. This explains why the helical swimmer turned towards the counter clockwise direction for the 180° angle direction steering.

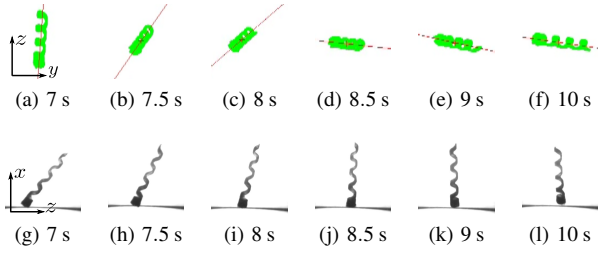

Fig. 6: Images sequence of 90° angle direction steering with 45° inclination angle. (a)-(f) show the top view of the helical swimer, and (g)-(l) show the side view.

3) Inclination angle of 65°*:* The direction steering of the helical swimmer was tested with even higher inclination angle like 65°. The characteristics of direction steering responses with a 65° inclination angle are similar as those with a 45° inclination angle. Their response times are summarized in Table II. It shows that the direction steering with a 65° inclination angle is more efficient than with a 45° inclination angle. Increasing the inclination angle of helical swimmer can not only increase the propulsive force in upward direction, but also increase the efficiency of the direction steering.

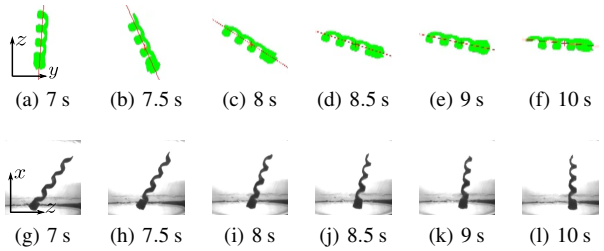

Fig. 7: Images sequence of −90° angle direction steering with 45° inclination angle. (a)-(f) show the top view of the helical swimmer, and (g)-(l) show the side view.

B. Inclination steering characterization

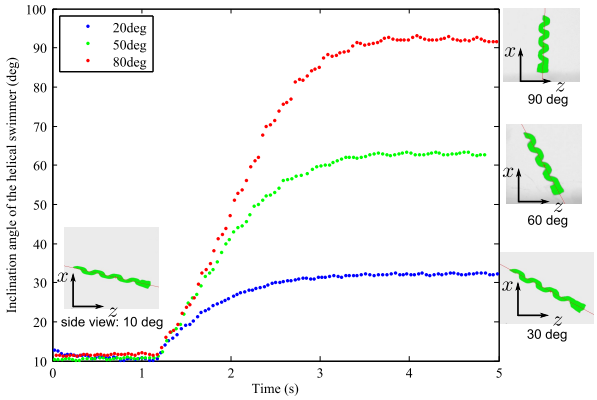

Fig. 8: Step responses of 20°, 50°, and 80° angle inclination steering. The initial inclination angle was 10°.

The inclination steering was studied with the direction angle kept at 0°. The helical swimmer was floating in the liquid at 3 Hz with an initial inclination angle of 10°. After 1 s, steering commands of 20°, 50°, and 80° were given. The inclination angle of the helical swimmer should end at 30°, 60°, 90° at the end of the steering. Fig. 8 shows the step responses of the 20°, 50°, and 80° angle inclination steering. All the responses exhibit first order system characteristics.

We developed a 3D steering strategy by combining inclination and direction steering. If the magnetic torque is not sufficient to steer the direction angle of the helical swimmer, we can at first increase its inclination angle, and then steer it. The optimal inclination angle which leads to the best steering performance in terms of response time will be studied in future works.

C. Steering on a sticky substrate

Floating conditions are ideal swimming conditions. If the generated propulsive force in the upward direction is not

enough to balance the gravity of the helical swimmer, it will sink down onto the substrate. At the microscale, the surface forces are important. Therefore, we use a sticky substrate, such as PDMS (Polydimethylsiloxane), to simulate high surface friction.

TABLE III: Response times of direction steering of the helical swimmer with different inclination angles on PDMS (unit: s).

Inclination angle	Command angle of direction steering			
	30°	90°	180°	-90°
0°	7.8	∞	-	∞
45°	4.0	6.9	8.5	5.6
65°	2.7	5.6	4.6	3.9

Table III summarizes the response times for 30°, 90°, 180°, and -90° angle direction steering on a PDMS substrate. The response time of the 30° angle direction steering with a 0° inclination angle on PDMS is much greater than that in floating conditions, which reveals that the steering performance is limited by high surface friction. The direction steering performances are greatly improved by increasing the inclination angle of the helical swimmer.

The 90° angle direction steering of the helical swimmer with a 0° inclination angle did not succeed because the magnetic torque was not strong enough. By the use of the proposed 3D steering strategy, we first increased the inclination angle to 45°. Then, the 90° angle direction steering was achieved. We predict that this strategy can improve steering performances at the microscale.

V. Conclusion

In this paper, we characterized the direction and inclination steering of a helical swimmer, by its orientation responses to step angle steering commands using real-time visual tracking of its orientation. The helical morphology is advantageous for linear propulsion but disadvantageous for steering performances due to the increased surface friction and interaction from the high surface to volume ratio. The steering performance characterizations clearly revealed that the direction steering performance of a helical swimmer was improved in terms of response time by increasing its inclination angle both in floating conditions and on a sticky substrate. Therefore, we proposed a 3D steering strategy by combing inclination and direction steering to improve the steering performance. This strategy was tested for a 90° angle direction steering with a 0° initial inclination angle. We predict that this strategy can help improve the steering performance for helical swimmers at the microscale. We further expect that the characterizations of steering performance can contribute to define the control parameters for future closed-loop control.

Acknowledgment

We acknowledge funding from Émergence-UPMC-2013 research program, the Franche-Comté region, and ANR Labex action ANR-11-LABX-01-01.

References

[1] L. Zhang, J.J. Abbott, L. Dong, B.E. Kratochvil, D. Bell, and B.J. Nelson. Artificial bacterial flagella: Fabrication and magnetic control. *Appl. Phys. Lett.*, 94(6), 2009.

[2] T. Truper, A. Kortschack, M. Jahnisch, H. Hulsen, and S. Fatikow. Transporting cells with mobile microrobots. *Nanobiotechnology, IEE Proceedings* -, 151(4):145–150, 2004.

[3] S. Tottori, L. Zhang, F. Qiu, K. Krawczyk, A. Franco-Obregn, and B.J. Nelson. Magnetic helical micromachines: Fabrication, controlled swimming, and cargo transport. *Advanced Materials*, 24(6):pp. 811–816, February 2012. highlighted as the front cover.

[4] N. Chaillet and S. Régnier. *Microrobotics for Micromanipulation*. ISTE. Wiley, 2013.

[5] B.J. Nelson, I.K. Kaliakatsos, and J.J. Abbott. Microrobots for minimally invasive medicine. *Annual Review of Biomedical Engineering*, 12(1):55–85, 2010.

[6] K.E. Peyer, L. Zhang, and B.J. Nelson. Bio-inspired magnetic swimming microrobots for biomedical applications. *Nanoscale*, 5(4):pp. 1259–1272, 2013.

[7] E.M. Purcell. Life at low reynolds number. *American Journal of Physics*, 45(1):3–11, 1977.

[8] E. Lauga and T.R. Powers. The hydrodynamics of swimming microorganisms. *Reports on Progress in Physics*, 72(9):096601, 2009.

[9] J.J. Abbott, M. Cosentino Lagomarsino, L. Zhang, L. Dong, and B.J. Nelson. How should microrobots swim? *The International Journal of Robotics Research*, 28(11-12):1434–1447, 2009.

[10] H.C. Berg and R.A. Anderson. Bacteria swim by rotating their flagellar filaments. *Nature*, 245(5425):380–382, 1973.

[11] T. Honda, K.I. Arai, and K. Ishiyama. Micro swimming mechanisms propelled by external magnetic fields. *Magnetics, IEEE Transactions on*, 32(5):5085 –5087, sep 1996.

[12] K. Ishiyama, K.I. Arai, M. Sendoh, and A. Yamazaki. Spiral-type micro-machine for medical applications. In *Micromechatronics and Human Science, 2000. MHS 2000. Proceedings of 2000 International Symposium on*, pages 65 –69, 2000.

[13] D.J. Bell, S. Leutenegger, K.M. Hammar, L.X. Dong, and B.J. Nelson. Flagella-like propulsion for microrobots using a nanocoil and a rotating electromagnetic field. In *Robotics and Automation, 2007 IEEE International Conference on*, pages 1128 –1133, april 2007.

[14] L. Zhang, J.J. Abbott, L. Dong, K.E. Peyer, B.E. Kratochvil, H. Zhang, C. Bergeles, and B. J. Nelson. Characterizing the swimming properties of artificial bacterial flagella. *Nano Letters*, 9:3663–3667, October 2009.

[15] L. Zhang, K.E. Peyer, and B.J. Nelson. Artificial bacterial flagella for micromanipulation. *Lab Chip*, 10:2203–2215, 2010.

[16] Ambarish Ghosh and Peer Fischer. Controlled propulsion of artificial magnetic nanostructured propellers. *Nano Letters*, 9(6):2243–2245, 2009.

[17] G. Hwang, S. Haliyo, and S. Régnier. Remotely powered propulsion of helical nanobelts. In *Robotics Science and Systems*, 2010.

[18] G. Hwang, R. Braive, L. Couraud, A. Cavanna, O. Abdelkarim, I. Robert-Philip, A. Beveratos, I. Sagnes, S. Haliyo, and S. Régnier. Electro-osmotic propulsion of helical nanobelt swimmers. *The International Journal of Robotics Research*, 30(7):806–819, 2011.

[19] Arthur W. Mahoney, John C. Sarrazin, Eberhar Bamberg, and Jake J. Abbott. Velocity control with gravity compensation for magnetic helical microswimmers. *Advanced Robotics*, 25(8):1007–1028, 2011.

[20] T. Xu, G. Hwang, N. Andreff, and S. Régnier. Scaled-up helical nanobelt modeling and simulation at low reynolds numbers. In *ICRA'12 IEEE International Conference on Robotics and Automation*, pages 4045 – 4051, 2012.

[21] T. Xu, G. Hwang, N. Andreff, and S. Regnier. Modeling and swimming property characterizations of scaled-up helical microswimmers, 2013.

[22] D. Jiles. *Introduction to magnetism and magnetic materials; 2nd ed.* Chapman and Hall, Boca Raton, FL, 1998.

[23] E. Marchand, F. Spindler, and F. Chaumette. Visp for visual servoing: a generic software platform with a wide class of robot control skills. *Robotics Automation Magazine, IEEE*, 12(4):40 –52, dec. 2005.

[24] B.K. Horn. *Robot Vision*. The MIT Press McGraw-Hill Higher Education, 1st edition, 1986.